Polymer Chemistry

PAPER

View Article Online
View Journal

Cite this: DOI: 10.1039/c8py01221k

Fabrication of theranostic amphiphilic conjugated bottlebrush copolymers with alternating heterografts for cell imaging and anticancer drug delivery†

Fangjun Liu,‡[a] Xuezhi Zhao,‡[a] Xiaolong Zhang,[a] Xianshuo Zhang,[a] Jinlei Peng,[a] Huiru Yang,[a] Kaicheng Deng,[a] Liwei Ma,[a] Cong Chang*[b] and Hua Wei *[a]

Received 19th August 2018,
Accepted 27th August 2018

DOI: 10.1039/c8py01221k

rsc.li/polymers

Bottlebrush (*bb*) copolymers with hetero-polymer grafts represent an intriguing advanced macromolecular architecture due to the unique phase-separation of the pendant side chains for polymer self-assembly and various functionalizations. However, compared to the well-developed polyfluorene (PF)-backboned *bb* copolymers with homobrushes, the incorporation of heterobrushes remains unexplored likely due to the synthetic challenges. For this purpose, we reported in this study the synthesis of a series of well-defined amphiphilic conjugated *bb* copolymers, PF-((*g*-PCL-OOCCH$_3$)-*alt*-(*g*-POEGMA)) with alternating poly(oligo(ethylene glycol)monomethyl ether methacrylate) (POEGMA)/poly(ε-caprolactone) (PCL) grafts, by integrated state-of-the-art polymer chemistry techniques including Suzuki-coupling polycondensation, ring-opening polymerization (ROP), click reaction and atom transfer radical polymerization (ATRP). One identified polymer construct (P_4) was able to form stabilized unimolecular micelles in an aqueous solution with a diameter of approximately 68 nm and showed the highest fluorescence quantum yield of 0.55, which is on a par with that of the small organic molecular fluorophore standard, quinine sulfate. The potential of P_4 for simultaneous cell imaging and drug delivery was further evaluated *in vitro*, which confirmed efficient cellular uptake and cytotoxicity in HeLa cells. This study thus presents the first example of PF-backboned *bb* copolymers with alternating heterobrushes for cancer theranostics.

Introduction

Polymers with advanced topological structures such as star-shaped polymers,[1–3] hyperbranched polymers,[4–9] cyclic polymers,[10–12] and bottlebrush (*bb*) polymers[13–25] show unique properties relative to their traditionally linear analogues with an identical molecular weight (MW), such as a smaller hydrodynamic radius, multi-valent polymer surface toward more functionalities, no or lower chain entanglement, and capability to form unimolecular micelles with greater stability; thus the design and precise synthesis of these polymers for various potential applications have been a hot subject of research for several decades and have drawn increasing attention in recent years. Among these structures, *bb* polymers with densely grafted polymer brushes represent an intriguing advanced macromolecular architecture due to the greater stability and drug loading capacity of their self-assembled micelles than those of their linear counterparts toward minimized side effects and enhanced therapeutic efficiency for drug delivery.[14,16,17,25–27] Compared to the extensive and intensive investigations on *bb* copolymers composed of homogeneous polymer brushes,[10–12] the preparation of *bb* copolymers with heterogeneous polymer grafts[17] remains relatively unexplored likely due to the synthetic challenge. *bb* copolymers with hetero-polymer brushes can self-assemble into more complex nanoassemblies including multi-compartment micelles and Janus-type cylinders with tunable functions and properties in selective solvents due to the unique phase separation of the pendant side chains with different properties. Therefore this self-assembly process of polymer species integrating two or more hetero-polymer brushes provides new insights into the properties of macromolecules with advanced topologies as well as their potential for various applications.[17] Together with the elegant adoption of functional polymers, *e.g.*, conjugated polymers as the backbone, the resulting *bb* copoly-

[a]State Key Laboratory of Applied Organic Chemistry, Key Laboratory of Nonferrous Metal Chemistry and Resources Utilization of Gansu Province, and College of Chemistry and Chemical Engineering, Lanzhou University, Lanzhou, Gansu 730000, China. E-mail: weih@lzu.edu.cn

[b]Department of Pharmaceutics, School of Pharmacy, Hubei University of Chinese Medicine, Wuhan, Hubei 430065, China. E-mail: 1126@hbtcm.edu.cn

†Electronic supplementary information (ESI) available. See DOI: 10.1039/c8py01221k

‡These authors contributed equally to this paper.

mers integrate simultaneously the abilities of cell-imaging for diagnosis and drug release for therapy.[13,15,20,22]

Polyfluorene (PF) is one of the most investigated conjugated polymers with superior fluorescence properties and both chemical and thermal stabilities.[28–47] More importantly, the C9 position of PF could be easily modified with a variety of functional groups, thus offering endless possibilities for chemistry decorations and biomedical applications.[35,37,42–47] Liu *et al.* synthesized a conjugated polyelectrolyte with pendant oligopeptide brushes using a facile strategy of click chemistry.[22] Wang *et al.* prepared a series of amphiphilic conjugated *bb* copolymers with the backbone of fluorescent poly(fluorene-*alt*-(4,7-bis (hexylthien)-2,1,3-benzothiadiazole)) (PFTB) grafted by the side chains of amphiphilic poly(ε-caprolactone)-*block*-poly(oligo (ethylene glycol)methyl ether methacrylate) (PCL-*b*-POEGMA) copolymers.[15] However, compared to the well-developed PF-backboned *bb* copolymers with homobrushes,[13,15,20–24] the incorporation of heterobrushes remains unexplored likely due to the synthetic challenges. For this purpose, we reported in this study the synthesis of a series of well-defined amphiphilic conjugated *bb* copolymers, PF-((*g*-PCL-OOCCH$_3$)-*alt*-(g-POEGMA)) (Scheme 1). The resulting amphiphilic conjugated *bb* copolymers are composed of not only a PF backbone with strong blue fluorescence for cell imaging, but also alternating POEGMA/PCL brushes capable of preventing the conjugated backbone from aggregation toward increased fluorescence quantum yields of PF. The potential of this formulation for simultaneous cell imaging and drug delivery was further evaluated *in vitro* by fluorescence microscopy and *in vitro* cytotoxicity study.

Results and discussion

Synthesis and characterization of PF-((*g*-PCL-OOCCH$_3$)-*alt*-(*g*-POEGMA)) copolymers

Well-defined amphiphilic conjugated *bb* copolymer PF-((*g*-PCL-OOCCH$_3$)-*alt*-(*g*-POEGMA)) was prepared in four steps including (a) synthesis of the PF backbone with alternating azide and hydroxyl functions in the termini of the pendant grafts, PF-((*g*-N$_3$)-*alt*-(*g*-OH)) (Scheme 2a), (b) synthesis of alkyne-PCL-OH by Sn(Oct)$_2$-catalyzed ROP of ε-CL using propynol as an initiator, and subsequent end capping of the reactive hydroxyl group to unreactive acetate by esterification (Scheme 2b), (c) conjugation of PCL grafts to the PF backbone by click coupling between PF-((*g*-N$_3$)-*alt*-(*g*-OH)) and alkyne-PCL-OOCCH$_3$ with an azide and alkyne molar feed ratio of 1 : 0.85 (Scheme 3), and (d) introduction of ATRP initiating sites into the above polymers by an esterification reaction with excess 2-bromoisobutyryl bromide, and production of target amphiphilic conjugated *bb* copolymers PF-((*g*-PCL-OOCCH$_3$)-*alt*-(*g*-POEGMA)) by ATRP of OEGMA using a PF-((*g*-PCL-OOCCH$_3$)-*alt*-(*g*-Br)) multimacroinitiator (Scheme 3). The MW, degree of polymerization (DP) and polydispersity ($Đ_M$) of all the synthesized polymers are summarized in Table 1. Note that the MWs of the synthesized polymers determined by ^{1}H NMR analyses are estimations rather than accurate calculations as detailed in Table 1.

Fig. S4† presents the typical ^{1}H NMR spectra of alkynyl-PCL$_{30}$-OH and alkyne-PCL$_{30}$-OOCCH$_3$. The DP of CL (Fig. S4a†) was determined to be approximately 30 according to our previous NMR analyses.[2,31] The terminal hydroxyl group of PCL was next converted to acetate by a reaction with anhydrous acetic acid and oxalyl chloride to avoid its transformation to ATRP initiating sites for the generation of POEGMA brushes in the fourth step of polymer synthesis mentioned above. The full end-capping of the hydroxyl termini by acetate functions was confirmed by the appearance of a new methyl signal (peak g)

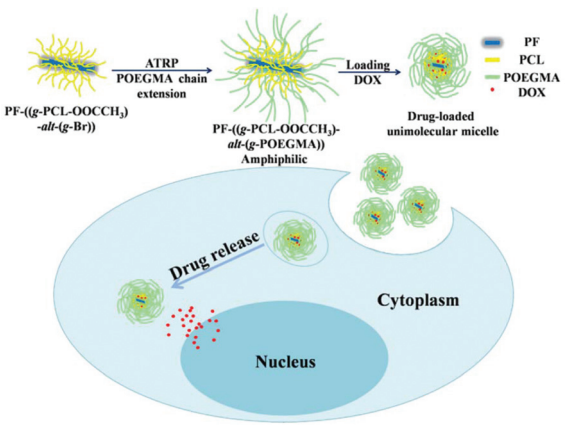

Scheme 1 Schematic representation of the synthesis, drug loading, cellular uptake, and intracellular drug release of the amphiphilic conjugated *bb* copolymers with alternating PCL/POEGMA grafts.

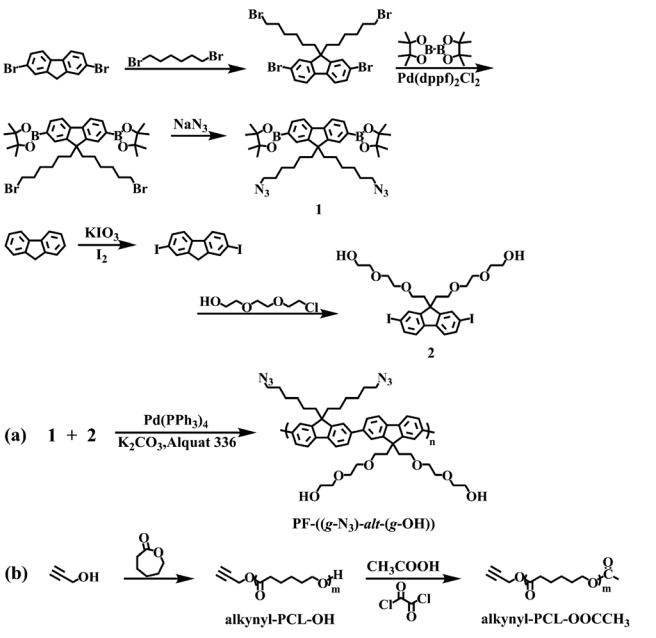

Scheme 2 Synthesis of monomers 2,7-bis(4,4,5,5-tetramethyl-1,3,2-dioxaborolan-2-yl)-9,9-bis(6′-azidohexyl)fluorine (**1**) and 2,7-diiodo-9,9-bis(2-(2-(2-hydroxyethoxy)ethoxy)ethyl)-fluorene (**2**), and polymers PF-((*g*-N$_3$)-*alt*-(*g*-OH)) (a) and alkynyl-PCL-OOCCH$_3$ (b).

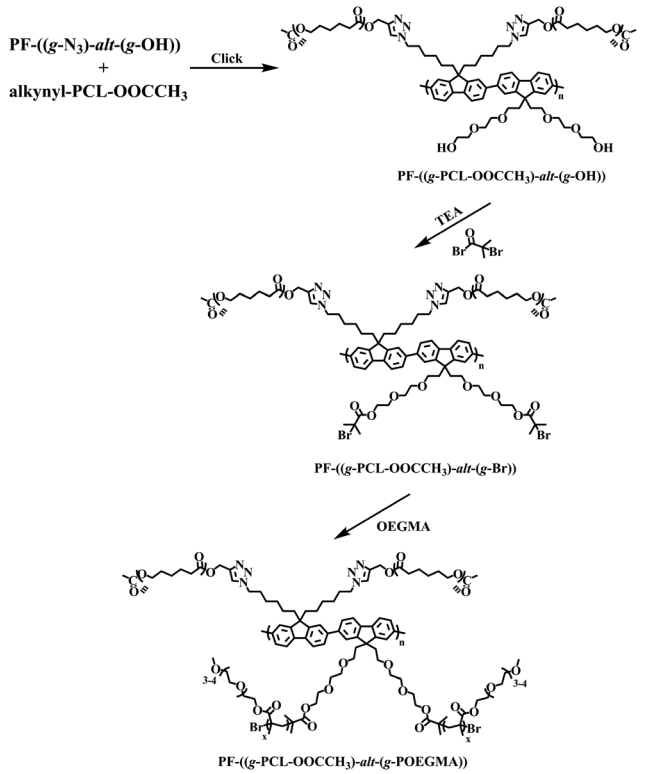

Scheme 3 Synthesis of *bb* copolymers PF-((*g*-PCL-$OOCCH_3$)-*alt*-(*g*-POEGMA)) *via* an integrated approach of "graft to" and "graft from".

at 2.04 ppm and a ratio of 2/3 of the integrated intensity of peak a (the methylene protons adjacent to alkynyl) to peak g (the protons of the methyl termini) (Fig. S4b†). The unimodal SEC elution peak with narrow distribution recorded for alkyne-PCL_{30}-$OOCCH_3$ demonstrates a well-controlled ROP process (Fig. 2a). The successful synthesis of the well-defined parent polymer of PF with alternating azide and hydroxyl functions in the termini of the pendant grafts, PF-((*g*-N_3)-*alt*-(*g*-OH)), through the Suzuki coupling reaction between monomer **1** (Fig. S1†) and monomer **2** (Fig. S2†), was confirmed by ^{1}H NMR and SEC-MALLS analyses (Fig. S3† and Fig. 2a). The resulting PF-((*g*-N_3)-*alt*-(*g*-OH)) also indicates a unimodal SEC elution peak with narrow distribution, and the DP of PF was determined to be ~13 based on the MW determined by SEC-MALLS.

The hydrophobic PCL grafts, alkyne-PCL_{30}-$OOCCH_3$, were subsequently conjugated to the parent PF, PF-((*g*-N_3)-*alt*-(*g*-OH)), by a copper(I)-catalyzed azide–alkyne cycloaddition (CuAAC) click reaction to generate the conjugated *bb* copolymer, PF_{13}-((*g*-PCL_{30}-$OOCCH_3$)-*alt*-(*g*-OH)). Note that the azide group was used in slight excess of the alkyne function with a molar feed ratio of 1 : 0.85 for simplified purification, taking advantage of the high efficiency of the CuAAC click-grafting. Successful polymer synthesis was confirmed by the appearance of all the characteristic signals of both PF and PCL moieties (Fig. 1a), a clear change of the signal at 3.15 ppm attributed to the methylene protons adjacent to azide in the ^{1}H NMR spectrum of PF-((*g*-N_3)-*alt*-(*g*-OH)) (Fig. S3†) to 4.20 ppm in the ^{1}H NMR spectrum of PF_{13}-((*g*-PCL_{30}-$OOCCH_3$)-*alt*-(*g*-OH)) (Fig. 1a) after click coupling as well as a notable shift of its SEC elution trace toward a higher MW relative to the parent polymer of PF (Fig. 2a). Moreover, the high purity of the synthesized PF_{13}-((*g*-PCL_{30}-$OOCCH_3$)-*alt*-(*g*-OH)) was corroborated by a complete shift of the resonance signal at 4.67 ppm attributed to the methylene protons adjacent to alkynyl in the ^{1}H NMR spectrum of alkyne-PCL_{30}-$OOCCH_3$ (Fig. S4a†) to 5.14 ppm in the ^{1}H NMR spectrum of PF_{13}-((*g*-PCL_{30}-$OOCCH_3$)-*alt*-(*g*-OH)) (Fig. 1a) after click grafting as well as its narrowly distributed SEC elution peak (Fig. 2a).

Next, the pendant hydroxyl groups of PF_{13}-((*g*-PCL_{30}-$OOCCH_3$)-*alt*-(*g*-OH)) were converted to ATRP initiators for generation of POEGMA brushes by a grafting-from approach. The successful introduction of ATRP initiating units was confirmed by a respective shift of the resonance signals at 3.64 and 3.49 ppm attributed to the protons of the methylene adjacent to the hydroxyl in the ^{1}H NMR spectrum of PF_{13}-((*g*-PCL_{30}-$OOCCH_3$)-*alt*-(*g*-OH)) (Fig. 1a) to 4.23 and 3.64 ppm (Fig. 1b) and the appearance of a new resonance signal (peak t) attributed to the methyl of the initiating units at 1.89 ppm in the ^{1}H NMR spectrum of PF_{13}-((*g*-PCL_{30}-$OOCCH_3$)-*alt*-(*g*-Br)) (Fig. 1b) after the reaction. Moreover, the ratio of the integrated intensity of peak t and peak (l + g) assigned to the protons of the methylene adjacent to 1,2,3-triazole and hydroxyl of PF_{13}-((*g*-PCL_{30}-$OOCCH_3$)-*alt*-(*g*-OH)) was calculated

Table 1 MW, $Đ_M$, and DP of all the synthesized polymers

Entry	Polymer[a]	$M_{n,\ NMR}$ [b] (kDa)	$M_{n,\ SEC\text{-}MALLS}$ [c] (kDa)	$Đ_M$ [c]
I_1	PF_{13}-((*g*-N_3)-*alt*-(*g*-OH))	—	11.4	1.38
I_2	Alkyne-PCL_{30}-OH	3.48	4.4	1.37
I_3	Alkyne-PCL_{30}-$OOCCH_3$	3.52	4.4	1.36
I_4	PF_{13}-((*g*-PCL_{30}-$OOCCH_3$)-*alt*-(*g*-OH))	89.8	72.4	1.52
I_5	PF_{13}-((*g*-PCL_{30}-$OOCCH_3$)-*alt*-(*g*-Br))	93.7	80.3	1.40
P_1	PF_{13}-((*g*-PCL_{30}-$OOCCH_3$)-*alt*-(*g*-$POEGMA_{12}$))	187.3	169.5	1.52
P_2	PF_{13}-((*g*-PCL_{30}-$OOCCH_3$)-*alt*-(*g*-$POEGMA_{18}$))	234.1	215.8	1.60
P_3	PF_{13}-((*g*-PCL_{30}-$OOCCH_3$)-*alt*-(*g*-$POEGMA_{23}$))	273.1	237.1	1.58
P_4	PF_{13}-((*g*-PCL_{30}-$OOCCH_3$)-*alt*-(*g*-$POEGMA_{38}$))	390.1	403.8	1.68

[a] The DP of the backbone PF_{13}-((*g*-N_3)-*alt*-(*g*-OH)) was calculated from SEC-MALLS results; the DP of PCL and POEGMA brushes was calculated from ^{1}H NMR results based on the DP of N_3-PF-OH. [b] $M_{n,\ NMR}$ was estimated from ^{1}H NMR results. [c] $M_{n,\ SEC\text{-}MALLS}$ was calculated from SEC-MALLS results.

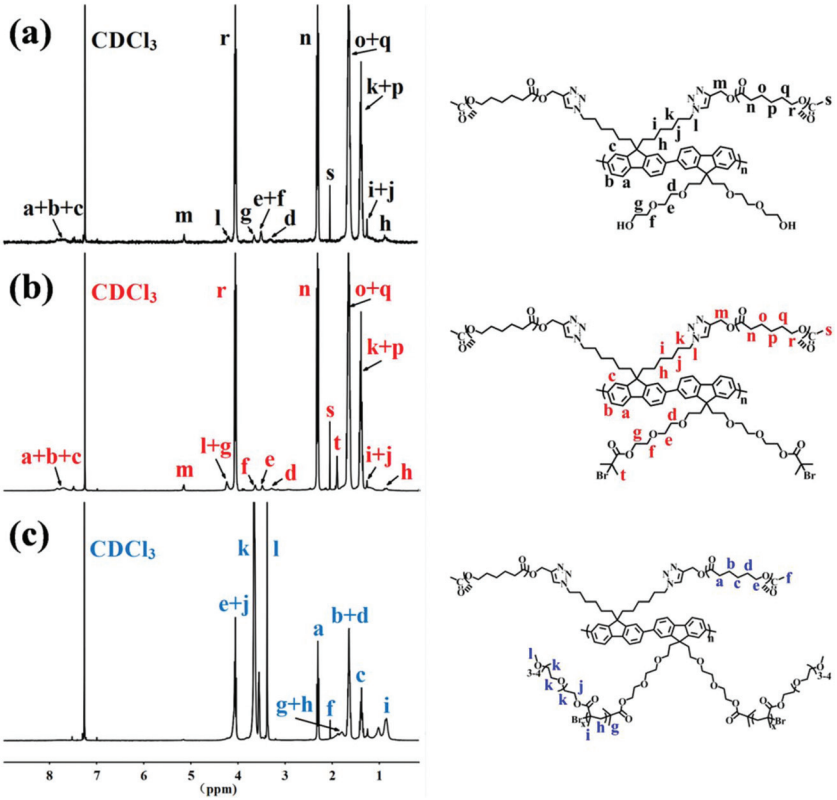

Fig. 1 ^{1}H NMR spectra of (a) PF_{13}-((*g*-PCL_{30}-$OOCCH_3$)-*alt*-(*g*-OH)), (b) PF_{13}-((*g*-PCL_{30}-$OOCCH_3$)-*alt*-(*g*-Br)), and (c) PF_{13}-((*g*-PCL_{30}-OOCCH3)-*alt*-(*g*-$POEGMA_{38}$)).

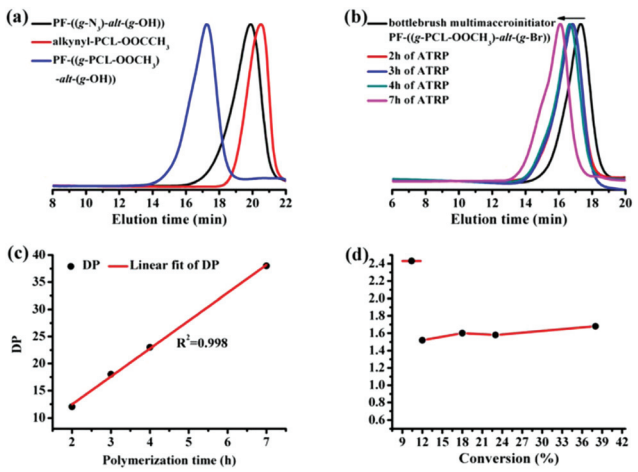

Fig. 2 SEC elution traces (dRI signals) of (a) PF_{13}-((*g*-N_3)-*alt*-(*g*-OH)), alkyne-PCL_{30}-$OOCCH_3$, and PF_{13}-((*g*-PCL_{30}-$OOCCH_3$)-*alt*-(*g*-OH)), (b–d) ATRP kinetics study of the conjugated *bb* copolymers using the PF_{13}-((*g*-PCL_{30}-$OOCCH_3$)-*alt*-(*g*-Br)) multimacroinitiator with a target DP of 100 for each initiating site.

to be 3/2, indicating complete decoration of the ATRP initiating sites.

The ATRP kinetic study using a PF_{13}-((*g*-PCL_{30}-$OOCCH_3$)-*alt*-(*g*-Br)) multimacroinitiator was carried out at various polymerization periods with a target DP of 100 for each initiating site. The SEC elution traces of the prepared four conjugated amphiphilic *bb* copolymers, PF-((*g*-PCL-$OOCCH_3$)-*alt*-(*g*-POEGMA)), show a detectable shift toward the higher MW with the polymerization time (Fig. 2b). During the evaluated polymerization process, the living characteristics were reflected by the pseudo-first-order kinetics and an almost constant $Đ_M$ around 1.60 (Fig. 2c & d). The acquired relatively broad $Đ_M$ relative to those of the linear polymers is reasonable given the more complicated polymer structure of *bb* copolymers and similar values reported in previous studies.[4,6,16,31,35] The DP of POEGMA brushes was calculated by comparing the integrated intensity of peak l at 3.38 ppm attributed to the protons of the methoxyl termini of POEGMA brushes and peak a assigned to the characteristic signal of PCL grafts (Fig. 1c).

Size and morphology of self-assembled micelles

The size of polymeric micelles is a critical factor that exerts a significant effect on the performance of micelle drug carriers. To achieve efficiently passive tumor targeting, the polymer micelles should have a relatively small size (<100 nm), which can guarantee a lower level of nonspecific uptake by the Reticuloendothelial System (RES), minimal renal excretion, and promotion of the enhanced permeability and retention (EPR) effect.[48,49] The ability of four amphiphilic conjugated *bb* copolymers PF_{13}-((*g*-PCL_{30}-$OOCCH_3$)-*alt*-(*g*-POEGMA)) (P_1–P_4)

to form unimolecular micelles was further evaluated using *N*,*N*′-dimethylformamide (DMF) as the medium that is a good solvent for all the moieties of the synthesized *bb* copolymers including the PF backbone, alternating brushes of PCL and POEGMA. Given the non-occurrence of self-assembly of the resulting *bb* copolymers in DMF, the mean size determined by dynamic light scattering (DLS) in DMF at a polymer concentration of 0.1 mg ml^{-1} reveals an actual dimension reached by a free polymer chain. On the other hand, self-assembly of the resulting *bb* copolymers in water takes place due to their amphiphilicity; therefore the average size determined by DLS in water at an identical polymer concentration of 0.1 mg ml^{-1} indicates a statistical diameter of the nano-objects self-assembled by the polymers. A close value of the two sizes supports the formation of unimolecular micelles consisting of a single polymer chain because association of polymer chains in an aqueous phase leads to a significantly larger size of the formed aggregates relative to that of a free polymer chain determined in DMF.

The mean size shows an increasing trend following the order of $P_4 > P_3 > P_2 > P_1$ in DMF (Table 2 and Fig. S5†), which indicates that the differences in the sizes of their self-assemblies are substantially dependent on the POEGMA brushes and the longer chain length of POEGMA brushes results in a larger dimension of a *bb* polymer chain because all the synthesized four amphiphilic conjugated *bb* copolymers have the same PF backbone and pendant hydrophobic PCL brushes but different chain lengths of hydrophilic POEGMA grafts. More importantly, it is interesting to notice that P_4 exhibits quite similar sizes in DMF and water (64.30 *vs.* 67.63 nm) at an identical polymer concentration of 0.1 mg mL^{-1} (Table 2), supporting its formation of unimolecular micelles in an aqueous solution. However, the other three polymers, P_1, P_2, and P_3, show a significantly greater size in water than those recorded in DMF likely due to the association of polymer chains with micelle structures for particulate stabilization. Therefore the trend of size recorded in water is quite different from the tendency observed in DMF. The diversities observed in the mean size determined in water are relevant to the dimension of a free polymer chain and the different aggregation numbers of the formed self-assemblies. The sizes of the self-assembled micelles are also affected by the parameters such as the molecular weight, polymer composition, concentration of solution and so on.[50] Such unique self-assembly behaviors of P_4 should be attributed to its longest POEGMA brushes among all the four *bb* copolymers. The strongest steric hindrance resulting from the longest POEGMA brushes of P_4 provides sufficient stability for its formation of unimolecular micelles rather than aggregates associated by the free polymer chains in water.

Transmission electron microscopy (TEM) was further performed to provide morphological insight into the self-assemblies formed by the amphiphilic conjugated *bb* copolymers (Fig. 3 & Fig. S6†), which reveals the formation of the well-dispersed micelles with a regular spherical shape for all the four *bb* copolymers. The average diameter of micelles self-assembled by P_3 and P_4 at a polymer concentration of 0.5 mg mL^{-1} was estimated to be approximately 42 and 28 nm, respectively, in water from the TEM images (Fig. 3c & d, the corresponding mean sizes determined by DLS are presented in Fig. 3a & b). To validate the unique formation of unimolecular micelles by P_4, TEM visualization was carried out in DMF as well. As expected, the average size of P_3 micelles in water is clearly larger than that observed in DMF (~21 nm from Fig. 3e). In contrast, P_4 micelles exhibit a mean size of ~30 nm in DMF (Fig. 3f) that is almost identical to the value determined in water. The results agree well with the DLS data and strongly support the greater stability of P_4 micelles relative to the other three micelle constructs due to the longest chain length of POEGMA brushes of P_4.

Various factors in the physiological systems, such as ionic strength, dilution with bloodstream and proteins, also exert a

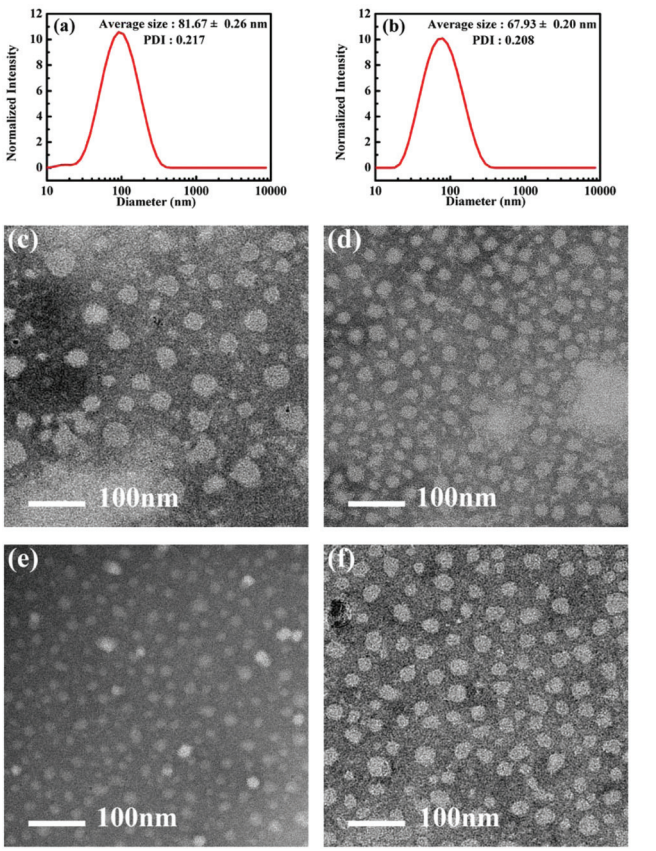

Fig. 3 Size distributions of (a) P_3 and (b) P_4 micelles in water, TEM images of (c & e) P_3 and (d & f) P_4 micelles in (c & d) water and (e & f) DMF at a polymer concentration of 0.5 mg mL^{-1}.

Table 2 Summary of the mean sizes and polydispersity indexes (PDIs) of the synthesized four amphiphilic *bb* copolymers, P_1–P_4, determined by DLS in water and DMF at a polymer concentration of 0.1 mg mL^{-1}

D_h (nm)$_{PDI}$	P_1	P_2	P_3	P_4
Water	$97.75_{/0.350}$	$77.39_{/0.218}$	$81.67_{/0.217}$	$67.63_{/0.208}$
DMF	$33.61_{/0.294}$	$37.45_{/0.222}$	$43.59_{/0.277}$	$64.30_{/0.324}$

significant effect on the structural integrity of the self-assembled micelles.[15,51] To evaluate the stability of micelles formed by P_3 and P_4 under salt and diluted conditions, the average diameter at various concentrations in different media was determined by DLS (Fig. S7a† & Fig. 4a). The average size of P_4 micelles remains almost identical in the tested polymer concentrations ranging from 0.1 to 2.0 mg mL^{-1} in both water and PBS (Fig. 4a), confirming the apparent stability of P_4 micelles irrespective of salt addition and dilution due to the formation of unimolecular micelles with enhanced stability. On the other hand, P_3 micelles showed consistently slightly smaller average diameters in water than those recorded in PBS likely due to the salt effect. Both values remain constant in the range of polymer concentrations from 0.05 to 1.0 mg mL^{-1}, also implying the stability of micelles under the physiological salt and diluted conditions (Fig. S7a†).

In vitro drug loading and drug release studies

To investigate the potential performance of the amphiphilic conjugated *bb* copolymers for drug delivery applications, *in vitro* drug loading and drug release studies were performed using doxorubicin (DOX) as the model drug. P_3 and P_4 micelles with enhanced stability were chosen to encapsulate DOX *via* a classical dialysis method to produce two theranostic micelles of DOX@P_3 and DOX@P_4.

After encapsulation of DOX within the hydrophobic core of the micelles, the average diameters of both drug-loaded micelles showed a slight increase (Fig. S7c† & Fig. 4c) relative to those of the blank micelles (Fig. S7b† & Fig. 4b) in PBS and (Fig. S7d† & Fig. 4d) in the presence of 10% fetal bovine serum (FBS), which demonstrates that drug encapsulation increases somewhat the micelle size. It is important to note that the DOX@P_4 micelles show a better symmetrical size distribution and a smaller PDI relative to the DOX@P_3 micelles, probably implying the greater stability of unimolecular micelles of P_4 relative to the micelles self-assembled by P_3. Such greater stability also contributed to the higher drug loading capacity of P_4 micelles, leading to slightly larger DLC and EE of DOX@P_4 micelles (4.2% and 46%) relative to DOX@P_3 analogues (3.8% and 42%).[31]

The *in vitro* DOX release profiles of the two theranostic micelles were investigated at 37 °C under the physiological conditions (PBS, pH 7.4, 150 mM) simulating the typical extracellular pH, and in an acidic medium (SSC, pH 5.0 150 mM) mimicking the tumor intracellular pH, respectively. As shown in Fig. 5, DOX release of DOX@P_4 micelles in the acidic medium of pH 5.0 was consistently faster than that recorded under the physiological conditions of pH 7.4, *i.e.*, 60% DOX release at pH 5.0 *vs.* 40% DOX release at pH 7.4 in 96 h (Fig. 5), which is primarily attributed to the promoted protonation of the glycosidic amine toward increased solubility of DOX in an acidic medium.[31] Based on the current results, both release profiles gradually levelled off after 48 h, approaching the "zero-order" kinetics.[52] Therefore a greater cumulative drug release could be achieved for a long-term drug release.

An identical trend of *in vitro* DOX release was observed for DOX@P_3 micelles, which mediated a slightly higher cumulative drug release at both pH values, *i.e.*, 65% at pH 5.0 and 46% at pH 7.4 in 72 h (Fig. S8†), than DOX@P_4 formulations, likely relevant to the differences in micelle stabilities.

Photophysical properties

The optical properties include the absorption and emission spectra, as well as the fluorescence quantum yields of conjugated polymers. It has been repeatedly highlighted that aggregation of conjugated polymers leads to significantly reduced fluorescence quantum yields. In this study, the phase-separation of the hetero-polymer brushes can prevent the PF backbone from aggregation and contribute to the increased fluorescence quantum yields of the synthesized four amphiphilic conjugated *bb* copolymers. To clarify the structure–property relationship, the photophysical properties of the synthesized four amphiphilic conjugated *bb* copolymers, P_1–P_4, were investigated in water and DMF at room temperature. All the poly-

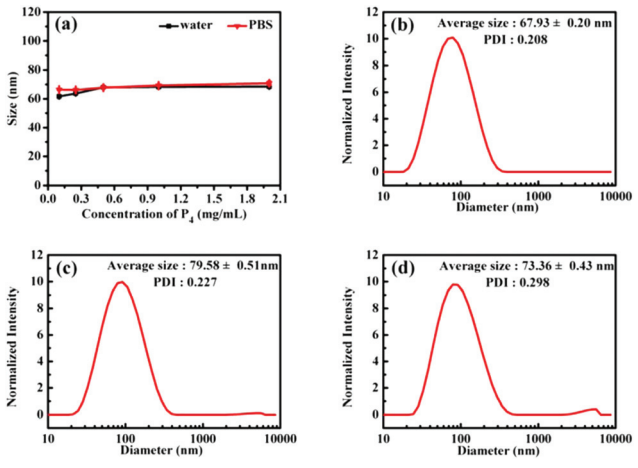

Fig. 4 Average sizes of P_4 at various concentrations in water and DMF determined by DLS, size distributions of (b) P_4 in PBS, (c) DOX@P_4 in PBS and (d) DOX@P_4 in the presence of 10% FBS at a polymer concentration of 1 mg mL^{-1}.

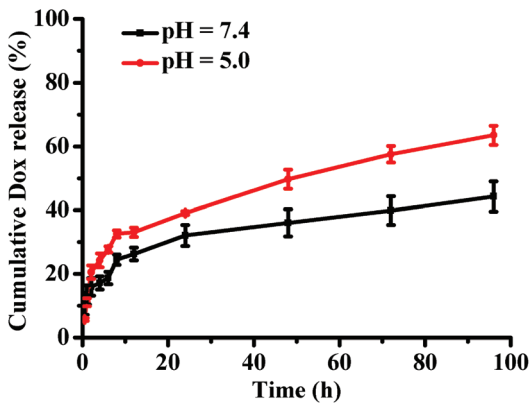

Fig. 5 *In vitro* drug release profiles of DOX@P_4 micelles at different pH values of 7.4 and 5.0 at 37 °C.

mers showed similar photophysical properties in both solvents (Fig. 6a, Fig. S9 & S10a†) with the typical absorption peak at 330–430 nm and the characteristic emission peak at 400–520 nm from the conjugated PF backbone when excited at 365 nm. The photophysical properties of DOX@P_3 and DOX@P_4 micelles were also investigated and compared to those of free DOX in water (Fig. 6b, Fig. S10b & S11†). There was a notable presence of the characteristic DOX absorption in the UV-Vis spectrum, but the emission spectrum of DOX was undetectable likely due to the excitation wavelength of 365 nm used for the PF moiety.

The fluorescence quantum yields of P_1–P_4 were calculated using quinine sulfate in 0.5 mol L^{-1} H_2SO_4 (Φ_F = 0.55) as the standard. The emission spectrum was recorded with an excitation wavelength of 365 nm. By comparing the integrated fluorescence spectrum of the polymers with that of quinine sulfate based on the correction of the refractive index differences in water and DMF, the fluorescence quantum yields of all the four *bb* copolymers in DMF were determined to be similar values (Table 3), but a significant increase of the fluorescence quantum yields from 0.35 to 0.55 in water was noticed following the order of $P_1 < P_2 < P_3 < P_4$ with increasing chain length of the hydrophilic POEGMA brushes from 12 to 38, which possibly implies that the longer POEGMA grafts provide better prevention of the PF backbone from aggregation and subsequent fluorescence quenching toward greater fluorescence properties. The photostability is reflected by the fluorescence quantum yields of polymers in water in this study.

Based on the results, P_4 micelles with the greater photostability than the other three micelles of P_1–P_3 were identified as the best polymer construct. The results agree well with the best stability of P_4 micelles. Most importantly, the fluorescence quantum yields of the unimolecular P_4 micelles in water are even as high as that of the quinine sulfate standard that is a small organic molecular fluorophore, confirming the great potential of P_4 micelles as a fluorescent probe for cellular imaging.

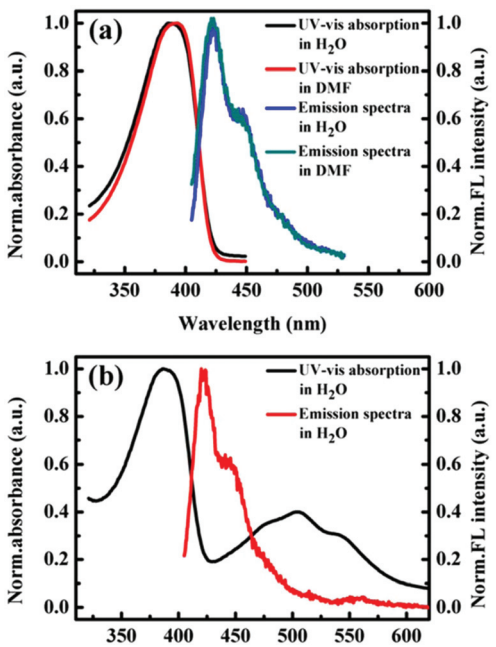

Fig. 6 UV-Vis absorption and fluorescence emission spectra of (a) P_4 in water and DMF and (b) DOX@P_4 in water.

Table 3 Summary of the photophysical properties of the four amphiphilic *bb* copolymers PF_{13}-((*g*-PCL_{30}-$OOCCH_3$)-*alt*-(*g*-POEGMA)) in water and DMF

Sample	Solvent	$\lambda_{max,\ abs}$ [a] (nm)	$\lambda_{max,\ em}$ [b] (nm)	Φ [c]
P_1	Water	386	423	0.35
P_1	DMF	393	419	0.75
P_2	Water	387	421	0.40
P_2	DMF	392	422	0.80
P_3	Water	388	423	0.51
P_3	DMF	391	422	0.73
P_4	Water	386	420	0.55
P_4	DMF	393	420	0.82

[a] The absorbance λ_{max} was determined from UV-Vis spectra. [b] The emission λ_{max} was determined from fluorescence spectra with excitation at 365 nm. [c] The fluorescence quantum yields of the amphiphilic *bb* copolymers in water and DMF were measured using quinine sulfate in 0.5 mol L^{-1} H_2SO_4 (Φ_F = 0.55) as the standard.

Cellular imaging and *in vitro* cytotoxicity

To evaluate the potential of DOX@P_3 and DOX@P_4 micelles in cellular imaging and drug delivery, the cellular uptake of micelles was observed by fluorescence microscopy. Note that HeLa cells were stained with acridine orange (AO) dye to distinguish the nuclei (Fig. 7b & Fig. S12,† indicated using arrows) from the cytoplasm stained in green. Taking the images of HeLa cells incubated with DOX@P_4 micelles as an example, the obvious blue fluorescence from the PF segment and the strong red fluorescence from DOX throughout the cellular cytoplasm and the perinuclear region (Fig. 7a & c), as well as the overlay image (Fig. 7d) confirm the efficient endocytosis of DOX@P_4 micelles into the cytoplasm of HeLa cells and their excellent abilities for cellular imaging and drug delivery. DOX@P_3 micelles showed similar cellular uptake behaviors (Fig. S12†).

Finally, the *in vitro* cytotoxicity of DOX@P_3 and DOX@P_4 micelles as well as the blank micelles was evaluated by the 3-(4,5-dimethylthiazol-2-yl)-5-(3-carboxymethoxyphenyl)-2-(4-sulfophenyl)-2*H*-tetrazolium (MTS) cell viability assay against HeLa cells (Fig. 8, Fig. S13 & S14†). The blank micelles of P_3 and P_4 are almost non-toxic to the cells, with a cell viability of 80% even at the highest tested polymer concentration of 2.6 mg mL^{-1} (Fig. S13†). The half maximal inhibitory concentration (IC_{50}) of free DOX, DOX@P_3 and DOX@P_4 micelles is 2.33 (2.27, 2.40) μg mL^{-1} (Fig. S15†), 89.44 (87.0, 101.5) μg mL^{-1} (Fig. S14†) and 87.60 (86.02, 110.3) μg mL^{-1} (Fig. 8), respectively. The DOX-loaded micelles exhibited significant cytotoxicity to HeLa cells, but had a less cytotoxic activity than free DOX likely due to the slower internalization mechanism (endocytosis *vs.* direct membrane permeation) and release

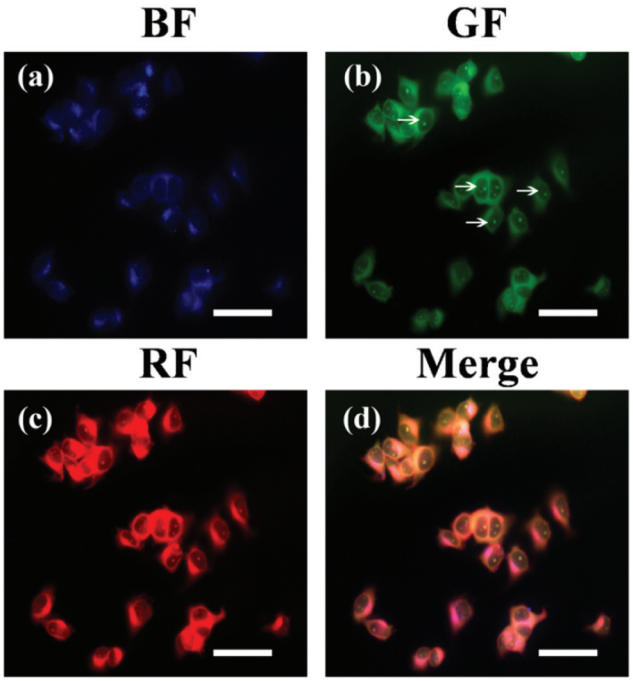

Fig. 7 Fluorescence microscopy images of DOX (red)-loaded P_4 (blue for the PF moiety) (DOX@P_4) micelle uptake in HeLa cells (cytoplasm stained green with acridine orange (AO)). Cells were treated with the polymer at 25% of its IC_{50} value to minimize cell death. The scale bar represents 50 μm.

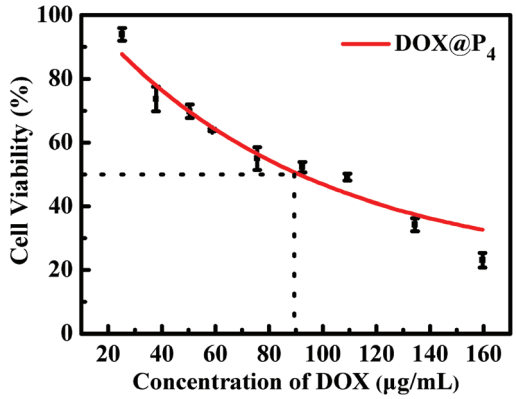

Fig. 8 *In vitro* cytotoxicity of DOX@P_4 micelles in HeLa cells.

kinetics of the free drug from the micelles.[31] The quite similar IC_{50} values of DOX@P_3 and DOX@P_4 micelles are attributed to the similar cumulative DOX release at pH 5.0.

Conclusions

In summary, we synthesized a series of amphiphilic conjugated *bb* copolymers with POEGMA/PCL heterografts by an integration of "grafting to" and "grafting from" techniques from the backbone of a PF-based parent polymer. P_4 was identified as the optimal polymer construct capable of forming stabilized unimolecular micelles in an aqueous solution with the highest fluorescence quantum yield of 0.55, which is on a par with that of the small organic molecular fluorophore standard, quinine sulfate. The potential of P_4 for simultaneous cell imaging and drug delivery was further evaluated *in vitro*, which confirmed efficient cellular uptake and cytotoxicity in HeLa cells. The current *bb* copolymers can be further modified with various strategies to develop multifunctional nanocarriers toward enhanced anticancer drug delivery, including (a) active targeting achieved by conversion of the bromo termini of POEGMA brushes to azide functions for further click coupling with various targeting ligands (*e.g.* antibody, peptide and small molecule ligand) and (b) efficient intracellular drug release realized by the introduction of different stimuli-responsive polymers as the pendant polymer brushes and/or incorporation of biorelevant cleavable links (*e.g.* reduction or acidic pH-sensitive bond) bridging the PF backbone and pendant polymer brushes.[8,9] Therefore the amphiphilic PF-backboned *bb* copolymers with hetero-polymer brushes developed herein present a promising alternative for cancer theranostics.

Conflicts of interest

There are no conflicts to declare.

Acknowledgements

The authors acknowledge the financial support from the National Natural Science Foundation of China (Grants 51473072 and 21504035), the Thousand Young Talent Program, the Open Research Fund of State Key Laboratory of Polymer Physics and Chemistry, Changchun Institute of Applied Chemistry, Chinese Academy of Sciences, and the Young Crop Plan of Hubei University of Traditional Chinese Medicine (2017ZZX021).

References

1 L. Zhao, C. F. Liu, W. D. Xu, Y. Jiang, W. Y. Lai and W. Huang, *J. Phys. Chem. B*, 2015, **119**, 6730–6739.
2 S. J. Zhao, H. R. Yang, C. Zuo, L. Sun, L. W. Ma and H. Wei, *RSC Adv.*, 2016, **6**, 111217–111225.
3 Y. Huang, F. Qiu, D. Chen, L. Y. Shen, S. T. Xu, D. B. Guo, Y. Su, D. Y. Yan and X. Y. Zhu, *Small*, 2017, **13**, 1604062.
4 H. R. Yang, X. Z. Zhao, X. L. Zhang, L. W. Ma, B. Y. Wang and H. Wei, *J. Polym. Sci., Part A: Polym. Chem.*, 2018, **56**, 1383–1394.
5 M. J. Zhang, H. H. Liu, W. Shao, K. Miao and Y. L. Zhao, *Macromolecules*, 2013, **46**, 1325–1336.
6 L. P. Zheng, Y. F. Wang, X. S. Zhang, L. W. Ma, B. Y. Wang, X. L. Ji and H. Wei, *Bioconjugate Chem.*, 2018, **29**, 190–202.
7 Z. Y. Feng, P. Tao, L. Zou, P. L. Gao, Y. Liu, X. Liu, H. Wang, S. J. Liu, Q. C. Dong, J. Li, B. S. Xu, W. Huang, W. Y. Wong

and Q. Zhao, *ACS Appl. Mater. Interfaces*, 2017, **9**, 28319–28330.
8 A. K. Pearce, B. E. Rolfe, P. J. Russell, B. W. C. Tse, A. K. Whittaker, A. V. Fuchsa and K. J. Thurecht, *Polym. Chem.*, 2014, **5**, 6932–6942.
9 A. V. Fuchs, A. P. Bapat, G. J. Cowin and K. J. Thurecht, *Polym. Chem.*, 2017, **8**, 5157–5166.
10 H. Wei, C. E. Wang, N. Tan, A. J. Boydston and S. H. Pun, *ACS Macro Lett.*, 2015, **4**, 938–941.
11 Y. F. Wang, Z. Z. Wu, Z. W. Ma, X. Y. Tu, S. J. Zhao, B. Y. Wang, L. W. Ma and H. Wei, *Polym. Chem.*, 2018, **9**, 2569–2573.
12 X. Y. Tu, C. Meng, X. L. Zhang, M. G. Jin, X. S. Zhang, X. Z. Zhao, Y. F. Wang, L. W. Ma, B. Y. Wang, M. Z. Liu and H. Wei, *Macromol. Biosci.*, 2018, **18**, 1800022.
13 H. Zhao, W. B. Hu, H. H. Ma, R. C. Jiang, Y. F. Tang, Y. Ji, X. M. Lu, B. Hou, W. X. Deng, W. Huang and Q. L. Fan, *Adv. Funct. Mater.*, 2017, **27**, 1702592.
14 Y. Y. Yuan, Q. Du, Y. C. Wang and J. Wang, *Macromolecules*, 2010, **43**, 1739–1746.
15 C. J. Yang, S. Huang, X. C. Wang and M. F. Wang, *Polym. Chem.*, 2016, **7**, 7455–7468.
16 M. Tong, X. N. An, W. D. Pan, H. H. Liu and Y. L. Zhao, *Polym. Chem.*, 2016, **7**, 2209–2221.
17 D. D. Tang, X. Jiang, H. H. Liu, C. X. Li and Y. L. Zhao, *Polym. Chem.*, 2014, **5**, 4679–4692.
18 Y. Shi, W. Zhu, D. D. Yao, M. L. Long, B. Peng, K. Zhang and Y. M. Chen, *ACS Macro Lett.*, 2014, **3**, 70–73.
19 S. S. Sheiko, B. S. Sumerlin and K. Matyjaszewski, *Prog. Polym. Sci.*, 2008, **33**, 759–785.
20 M. Madsen, R. S. Christensen, A. Krissanaprasit, M. R. Bakke, C. F. Riber, K. S. Nielsen, A. N. Zelikin and K. V. Gothelf, *Chem. – Eur. J.*, 2017, **23**, 10511–10515.
21 X. M. Lu, A. Wei, Q. L. Fan, L. H. Wang, P. Chen, X. C. Dong and W. Huang, *Mater. Res. Bull.*, 2012, **47**, 4335–4339.
22 J. Liu, G. G. Feng, J. L. Geng and B. Liu, *ACS Appl. Mater. Interfaces*, 2013, **5**, 4511–4515.
23 Q. Chen, Q. Y. Cheng, Y. C. Zhao and B. H. Han, *Macromol. Rapid Commun.*, 2009, **30**, 1651–1655.
24 A. Bolognesi, F. Galeotti, W. Mróz, V. Gancheva and L. Terlemezyan, *Macromol. Chem. Phys.*, 2010, **211**, 1488–1495.
25 D. Neugebauer, M. Theis, T. Pakula, G. Wegner and K. Matyjaszewski, *Macromolecules*, 2006, **39**, 584–593.
26 K. Miao, W. Shao, H. H. Liu and Y. L. Zhao, *Polym. Chem.*, 2014, **5**, 1191–1201.
27 H. H. Liu, C. X. Li, D. D. Tang, X. N. An, Y. F. Guo and Y. L. Zhao, *J. Mater. Chem. B*, 2015, **3**, 3959–3971.
28 C. L. Zhu, L. B. Liu, Q. Yang, F. T. Lv and S. Wang, *Chem. Rev.*, 2012, **112**, 4687–4735.
29 B. Zhu, Y. Han, M. H. Sun and Z. S. Bo, *Macromolecules*, 2007, **40**, 4494–4500.
30 H. Q. Zhong, C. C. Liu, W. J. Ge, R. C. Sun, F. Huang and X. H. Wang, *ACS Appl. Mater. Interfaces*, 2017, **9**, 22875–22884.
31 X. Z. Zhao, K. C. Deng, F. J. Liu, X. L. Zhang, H. R. Yang, J. L. Peng, Z. K. Liu, L. W. Ma, B. Y. Wang and H. Wei, *ACS Biomater. Sci. Eng.*, 2018, **4**, 566–575.
32 J. H. Yao, K. Y. Mya, L. Shen, B. P. He, L. Li, Z. H. Li, Z. K. Chen, X. Li and K. P. Loh, *Macromolecules*, 2008, **41**, 1438–1443.
33 S. H. Yang and C. S. Hsu, *J. Polym. Sci., Part A: Polym. Chem.*, 2009, **47**, 2713–2733.
34 L. Q. Xu, B. Zhang, R. Wang, Y. Chen, K. G. Neoh, E. T. Kang and G. D. Fu, *Polym. Chem.*, 2012, **3**, 2444.
35 R. Wang, W. Z. Wang, S. Lu and T. X. Liu, *Macromolecules*, 2009, **42**, 4993–5000.
36 J. Steverlynck, A. De Cattelle, J. D. Winter, P. Gerbaux and G. Koeckelberghs, *J. Polym. Sci., Part A: Polym. Chem.*, 2016, **54**, 1252–1258.
37 I. Meazzini, J. M. Behrendt, M. L. Turner and R. C. Evans, *Macromolecules*, 2017, **50**, 4235–4243.
38 F. T. Lv, T. Qiu, L. B. Liu, J. M. Ying and S. Wang, *Small*, 2016, **12**, 696–705.
39 A. Kaeser and A. P. Schenning, *Adv. Mater.*, 2010, **22**, 2985–2997.
40 V. İbrahimova, S. Ekiz, Ö. Gezici and D. Tuncel, *Polym. Chem.*, 2011, **2**, 2818–2824.
41 X. L. Feng, L. B. Liu, S. Wang and D. B. Zhu, *Chem. Soc. Rev.*, 2010, **39**, 2411–2419.
42 W. N. Zeng, S. P. Liu, H. X. Zou, L. Y. Wang, R. Beuerman and D. R. Cao, *J. Polym. Sci., Part A: Polym. Chem.*, 2010, **48**, 4168–4177.
43 L. Wu, I. C. Wu, C. C. DuFort, M. A. Carlson, X. Wu, L. Chen, C. T. Kuo, Y. L. Qin, J. B. Yu, S. R. Hingorani and D. T. Chiu, *J. Am. Chem. Soc.*, 2017, **139**, 6911–6918.
44 X. Q. Shen, L. Li, A. C. M. Chan, N. Y. Gao, S. Q. Yao and Q. H. Xu, *Adv. Opt. Mater.*, 2013, **1**, 92–99.
45 S. H. Oh, S. I. Na, Y. C. Nah, D. J. Vak, S. S. Kim and D. Y. Kim, *Org. Electron.*, 2007, **8**, 773–783.
46 C. Y. Nie, C. L. Zhu, L. H. Feng, F. T. Lv, L. B. Liu and S. Wang, *ACS Appl. Mater. Interfaces*, 2013, **5**, 4549–4554.
47 O. K. Nag, J. E. Jeong, T. L. Nguyen and H. Y. Woo, *Macromol. Res.*, 2015, **23**, 457–465.
48 M. Kanapathipillai, A. Brock and D. E. Ingber, *Adv. Drug Delivery Rev.*, 2014, **79–80**, 107–118.
49 S. D. Perrault, C. Walkey, T. Jennings, H. C. Fischer and W. C. W. Chan, *Nano Lett.*, 2009, **9**, 1909–1915.
50 W. Shao, K. Maio, H. H. Liu, C. N. Ye, J. Z. Du and Y. L. Zhao, *Polym. Chem.*, 2013, **4**, 3398–3410.
51 R. Savic, T. Azzam, A. Eisenberg and D. Maysinger, *Langmuir*, 2006, **22**, 3570–3578.
52 H. Wei, C. Cheng, C. Chang, W. Q. Chen, S. X. Cheng, X. X. Zhang and R. X. Zhuo, *Langmuir*, 2008, **24**, 4565–4570.